We are IntechOpen, the world's leading publisher of Open Access books
Built by scientists, for scientists

6,900
Open access books available

185,000
International authors and editors

200M
Downloads

154
Countries delivered to

Our authors are among the

TOP 1%
most cited scientists

12.2%
Contributors from top 500 universities

BOOK CITATION INDEX
CLARIVATE ANALYTICS
INDEXED

WEB OF SCIENCE™

Selection of our books indexed in the Book Citation Index
in Web of Science™ Core Collection (BKCI)

Interested in publishing with us?
Contact book.department@intechopen.com

Numbers displayed above are based on latest data collected.
For more information visit www.intechopen.com

Improving Tribological Behavior of Porous Anodic Film by Electrophoretic Impregnation by a Tio₂ Synthesized Nanoparticle

Koubaa Anouar and Bargui Mansour

Additional information is available at the end of the chapter

Abstract

This chapter deals with the study of the elaboration of a stable suspension of TiO_2 nanoparticles and their incorporation by electrophoretic deposition into pores of anodized 5754 aluminum alloy. The as-synthesized TiO_2 nanopowder was characterized by X-ray diffraction, scanning and transmission electron microscopy (TEM), and infrared spectroscopy. During this work, transmission electronic microscopy (TEM) analysis showed that the resulting particles had a narrow size distribution with crystallite size of about 15 nm. The zeta potential and stability of TiO_2 nanoparticles dispersed with poly(acrylic acid) (PAA) in aqueous solution were also measured. Porous anodic film was elaborated in phosphoric acid electrolyte and then filled by TiO_2 particles using electrophoresis method. Furthermore, the effect of PAA content and pH on the suspension stability has been investigated. It was also demonstrated that buffered suspension by adding glycine avoids gelating phenomena which inhibits the insertion of nanoparticles inside the pores of anodic film. It was noted also that the electric field already applied greatly influences the electrophoretic deposition process (EPD). FEG-SEM observations showed that larger (125 nm diameter) and linear pores of 6 μm in length are successfully filled in 5 min. Finally, the composite anodic film tribological behavior was studied and the obtained results revealed that the insertion of the TiO_2 nanoparticles into the pores of the anodic film improves its tribological properties.

Keywords: electrophoretic impregnation, anodizing, TiO_2 nanoparticles, zeta potential, colloidal suspension

1. Introduction

Nanotechnology is based on the knowledge and mastery of the infinitely small. They constitute a multidisciplinary field of research and development involving the fabrication of new materials and devices from tools or techniques that can be used to structure matter at the atomic, molecular, or supramolecular level. The typical scales of nanotechnology range from 1 to 100 nm.

The nanomaterials thus derived from these nanotechnologies are materials composed or constituted for all or part of nano-objects which confer to them improved or specific properties of the nanometric dimension. In this context, we speak of nanocharged or nanoreinforced materials. These materials are developed by incorporating nano-objects in an organic or mineral matrix to provide new functionality or to modify mechanical, optical, magnetic, or thermal properties. Nanocomposites are one example. Nano-objects (**Figure 1**) that have two different forms, nanotubes (e.g., MWNT: multi wall carbon nanotubes) or spherical particles (e.g., alumina powder) are incorporated in the porous matrix by several techniques, among which and the most interesting is that of electrophoresis. In this chapter, we are interested in presenting a work whose main objectives consisted in developing a model anodizing layer on the 5754 aluminum alloy, then a stable suspension of nanometric titanium dioxide, then composite coatings based on TiO_2 nanoparticles by electrophoretic impregnation of the anodizing layer, and finally rigorously examine the impact of TiO_2 localization on the tribological behavior of the composite coating already developed.
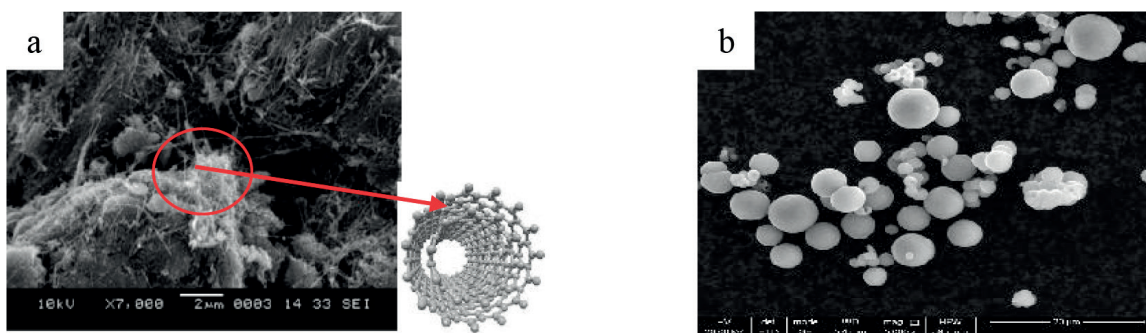

Figure 1. Different shapes of nano-objects (a) multi-wall carbon nanotubes and (b) spherical nanoparticles of alumina [1].

2. Protocol for incorporation of nanoparticles

The flowchart showed in **Figure 2** summarizes the range of the steps to be followed in order to prepare the model anodic film and fill its pores with nanoparticles of titanium dioxide.

2.1. Pretreatment: electropolishing

The electropolishing treatment was carried out in a bath already proposed by Sulka [2]. This pretreatment aims to reduce the roughness of the aluminum substrate. The results thus
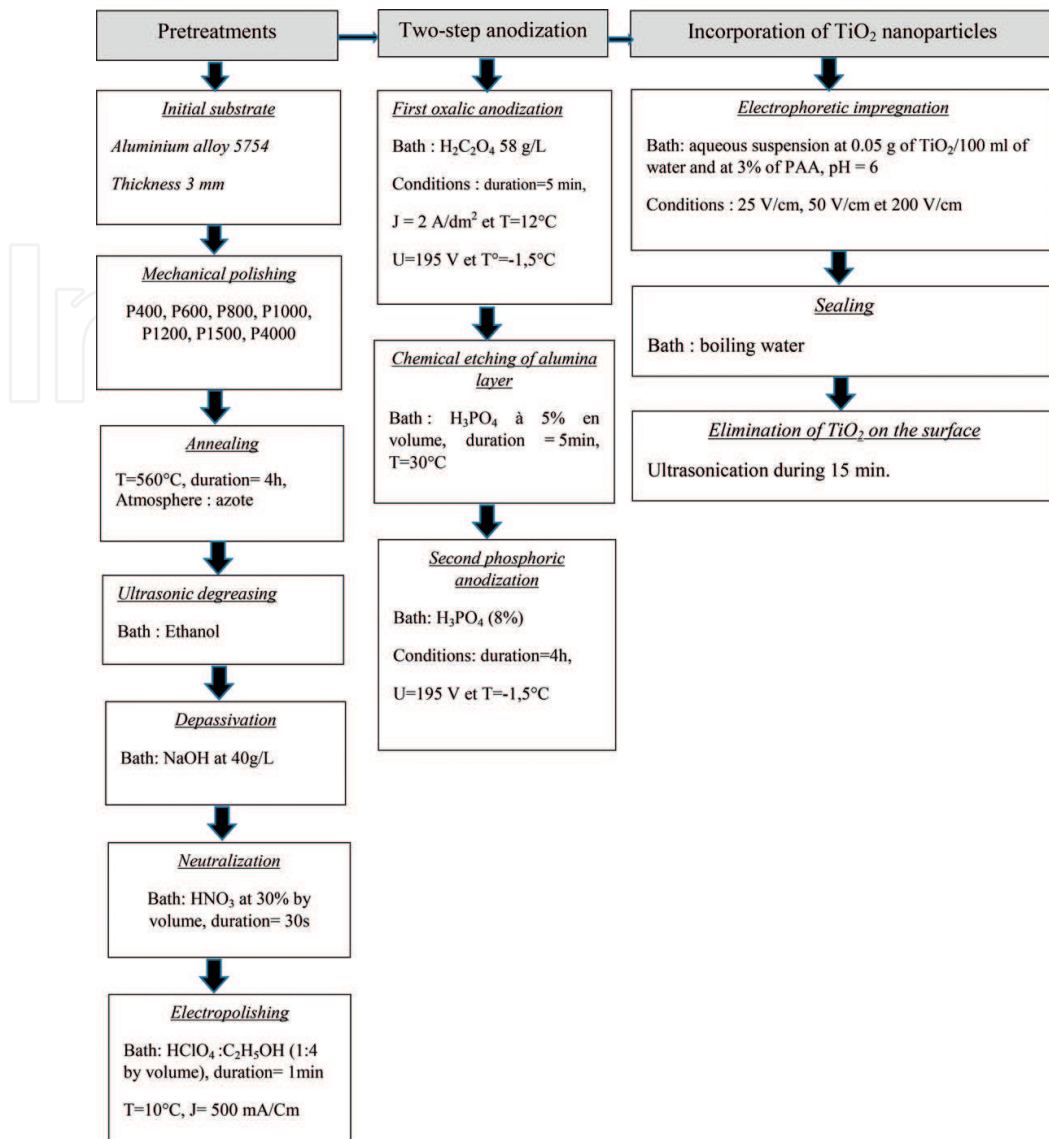
Pretreatments	Two-step anodization	Incorporation of TiO$_2$ nanoparticles
Initial substrate Aluminium alloy 5754 Thickness 3 mm	**First oxalic anodization** Bath : H$_2$C$_2$O$_4$ 58 g/L Conditions : duration=5 min, J = 2 A/dm^2 et T=12°C U=195 V et T°=-1,5°C	**Electrophoretic impregnation** Bath: aqueous suspension at 0.05 g of TiO$_2$/100 ml of water and at 3% of PAA, pH = 6 Conditions : 25 V/cm, 50 V/cm et 200 V/cm
Mechanical polishing P400, P600, P800, P1000, P1200, P1500, P4000	**Chemical etching of alumina layer** Bath : H$_3$PO$_4$ à 5% en volume, duration = 5min, T=30°C	**Sealing** Bath : boiling water
Annealing T=560°C, duration= 4h, Atmosphere : azote		**Elimination of TiO$_2$ on the surface** Ultrasonication during 15 min.
Ultrasonic degreasing Bath : Ethanol	**Second phosphoric anodization** Bath: H$_3$PO$_4$ (8%) Conditions: duration=4h, U=195 V et T=-1,5°C	
Depassivation Bath: NaOH at 40g/L		
Neutralization Bath: HNO$_3$ at 30% by volume, duration= 30s		
Electropolishing Bath: HClO$_4$:C$_2$H$_5$OH (1:4 by volume), duration= 1min T=10°C, J= 500 mA/Cm		

Figure 2. Incorporation flowchart of TiO$_2$ nanoparticles in the pores of anodic layer.

obtained are illustrated in **Figure 3**. Indeed the Al5754 aluminum substrate has an initial roughness (Ra = 740 nm and Rz = 7 μm) and a roughness after electrochemical polishing (Ra = 140 nm and Rz = 1.5 μm).

2.2. Two-step anodization

It should be noted that the anodization consists in carrying out the anodic polarization surface conversion of the base metal, immersed in a suitable electrolyte (generally an aqueous solution of a mineral acid). **Figure 4** shows an experimental setup of anodizing and the reactions that take place on the surfaces of the anode (Al5754) and the cathode.

Different kinds of electrolytes such as sulfuric acid, phosphoric acid, and oxalic acid can be used for anodization. Although sulfuric anodizing, which is nowadays the most commonly used process [3], phosphoric acid was used in the case of this study because it produces a
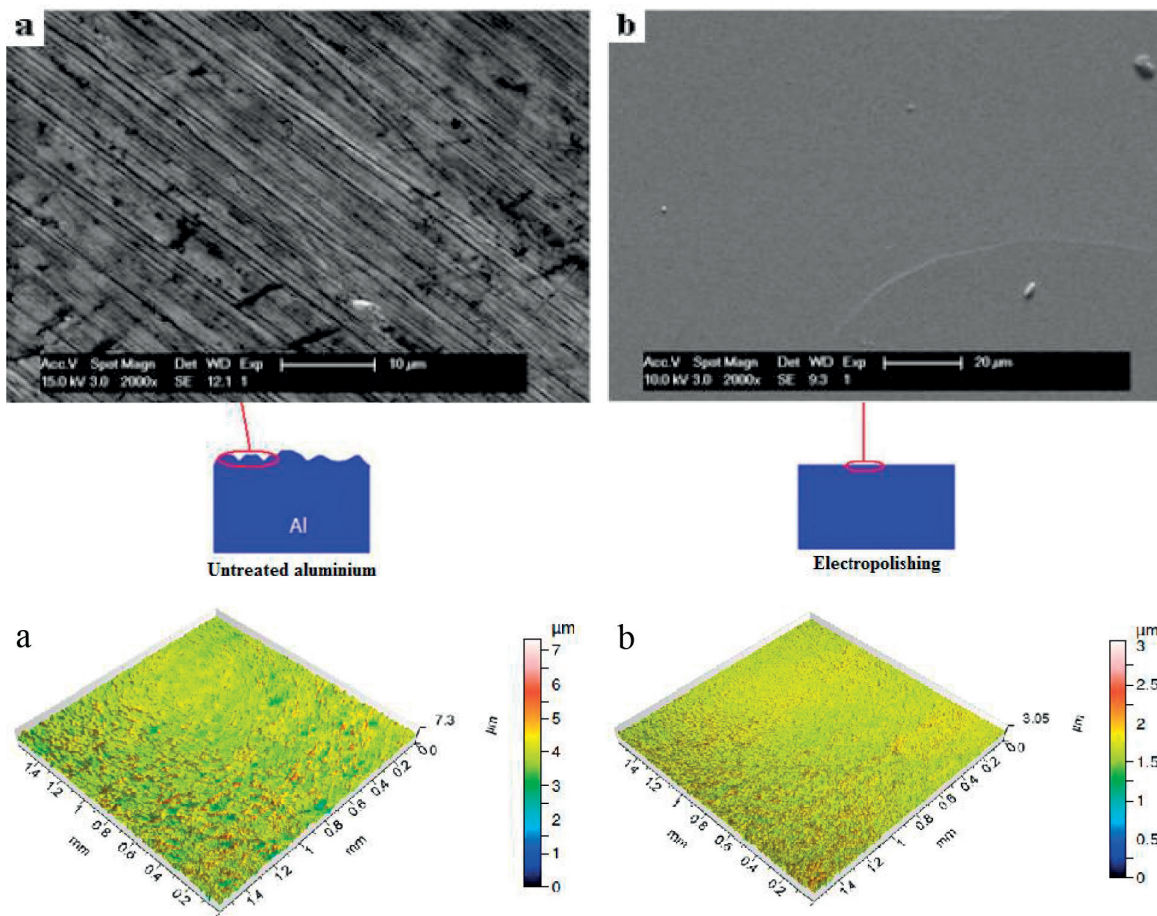
Figure 3. SEM observations associated with 3D roughness profiles: (a) sample after mechanical polishing and (b) after mechanical and electrochemical polishing.
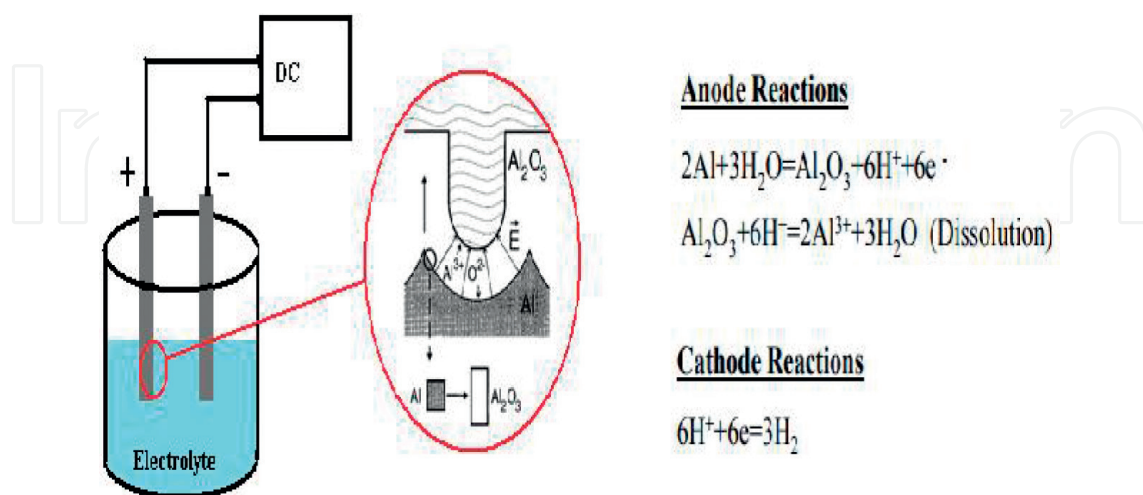

Anode Reactions

$$2Al+3H_2O=Al_2O_3+6H^++6e^-$$

$$Al_2O_3+6H^-=2Al^{3+}+3H_2O \ (Dissolution)$$

Cathode Reactions

$$6H^++6e=3H_2$$

Figure 4. Experimental setup of anodizing.

porous anodic layer with the largest pore diameter. The anodizing of aluminum has to be done by preference on samples with a low surface roughness then anodized according to the **two-step anodization** to obtain an ordered porous anodic film [4] with a pore diameter greater than 100 nm. **Figure 5** reveals the approach for the conduct of the two-step anodization and **Figure 6** shows the scanning electronic microscopy (SEM) images of the obtained anodic layer that can be impregnated with 20 nm size TiO_2 nanoparticles using **electrophoretic method**.

2.3. Electrophoretic impregnation of porous anodizing layer by synthesized TiO_2 nanoparticles

2.3.1. Synthesis of TiO_2 nanoparticles

In order to prepare the TiO_2 nanopowder, 10 ml of ethanol (C_2H_5OH), 10 ml of acetic acid (CH_3COOH), 400 μL of hydrochloric acid (HCL) were used as catalysts, and 10 ml of titanium tetraisopropoxide precursor(Ti $(OCH(CH_3)_2)_4$) were mixed in the indicated order. The mixture was stirred for 30 min at a constant speed of 200 rpm to obtain the TiO_2 sol. Then the resulting sol was introduced into the autoclave (**Figure 7**) heated up to 243°C and pressurized to overcome the critical point of ethanol (T_c = 243°C, P_c = 63 bar). After maintaining temperature at 243°C for 1 h, the sol-gelation occurred. To evacuate the interstitial solvent, depressurization for 1 h down to room temperature was conducted with nitrogen gas. Finally, titanium aerogel was obtained.

Figure 8 indicates the sol-gel TiO_2 fabrication diagram.

2.3.2. Structural and morphological investigations of TiO_2 nanopowder

Fourier-transform infrared (FTIR) spectroscopy was used to identify the functional groups presented in the as-synthesized TiO_2 nanopowder. The FTIR absorbance spectra were given
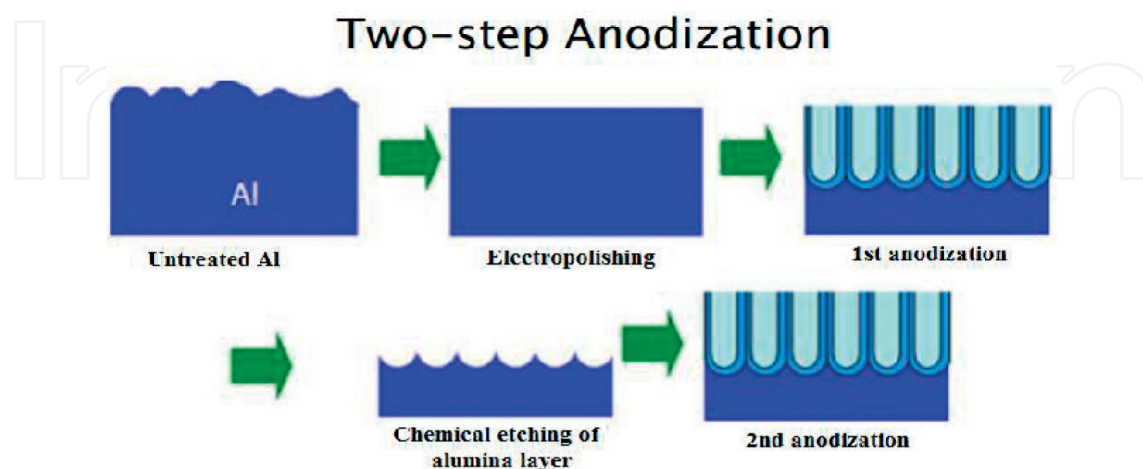

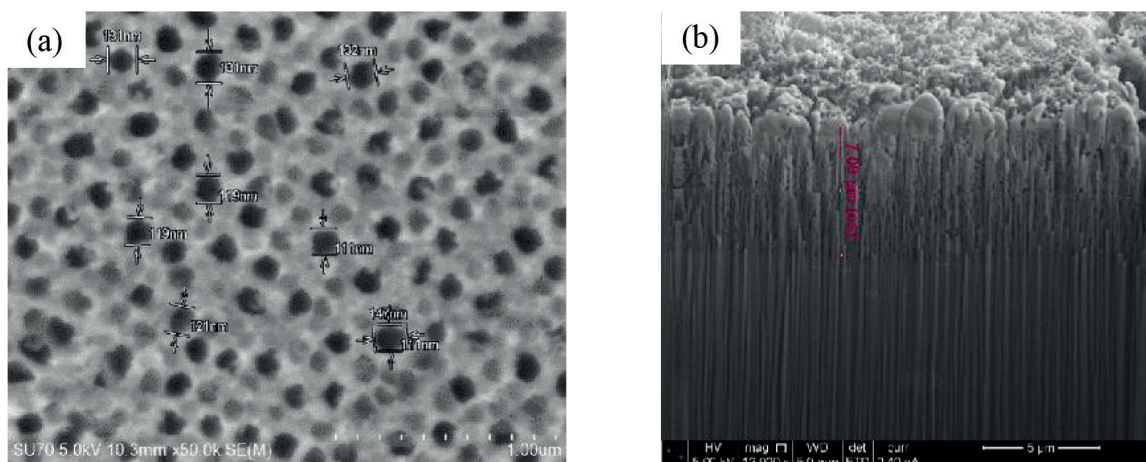**Figure 5.** The approach for the conduct of the two-step anodization.

Figure 6. SEM images of anodic layer elaborated on th Al5754 aluminum alloy (a) in phosphoric bath (H_3PO_4 8%, U = 195 V, T = −1.5° C and t = 4 h) and (b) cross section of the anodizing layer [5].

Figure 7. PARR autoclave-type pressure reactor and solvent removal system.

in **Figure 9**. A wide band ranging between 400 and 900 cm^{-1} was attributed to Ti-O stretching vibrations [6]. In the medium wavenumber range, the bands at 1300–1800 cm^{-1} were attributed to ν[C=C, C=O] and δ CH_3 vibrations corresponding to the organic residues [7]. It was believed that a broad band at ds 3500 cm^{-1} corresponds to the surface-adsorbed water [8]. In fact, the energy dispersive X-ray (EDX) spectra shown in **Figure 11** indicates the presence of an oxygen excess which can be attributed to the adsorbed hydroxide groups on the surface of TiO_2 nanoparticles.

The XRD pattern of TiO_2 nanopowder is shown in **Figure 10**. The obvious diffraction peaks of anatase TiO_2 structure in the range of resolution of XRD were well defined which indicated the good crystallinity of the synthesized TiO_2 nanopowder. In fact, the diffraction peaks at
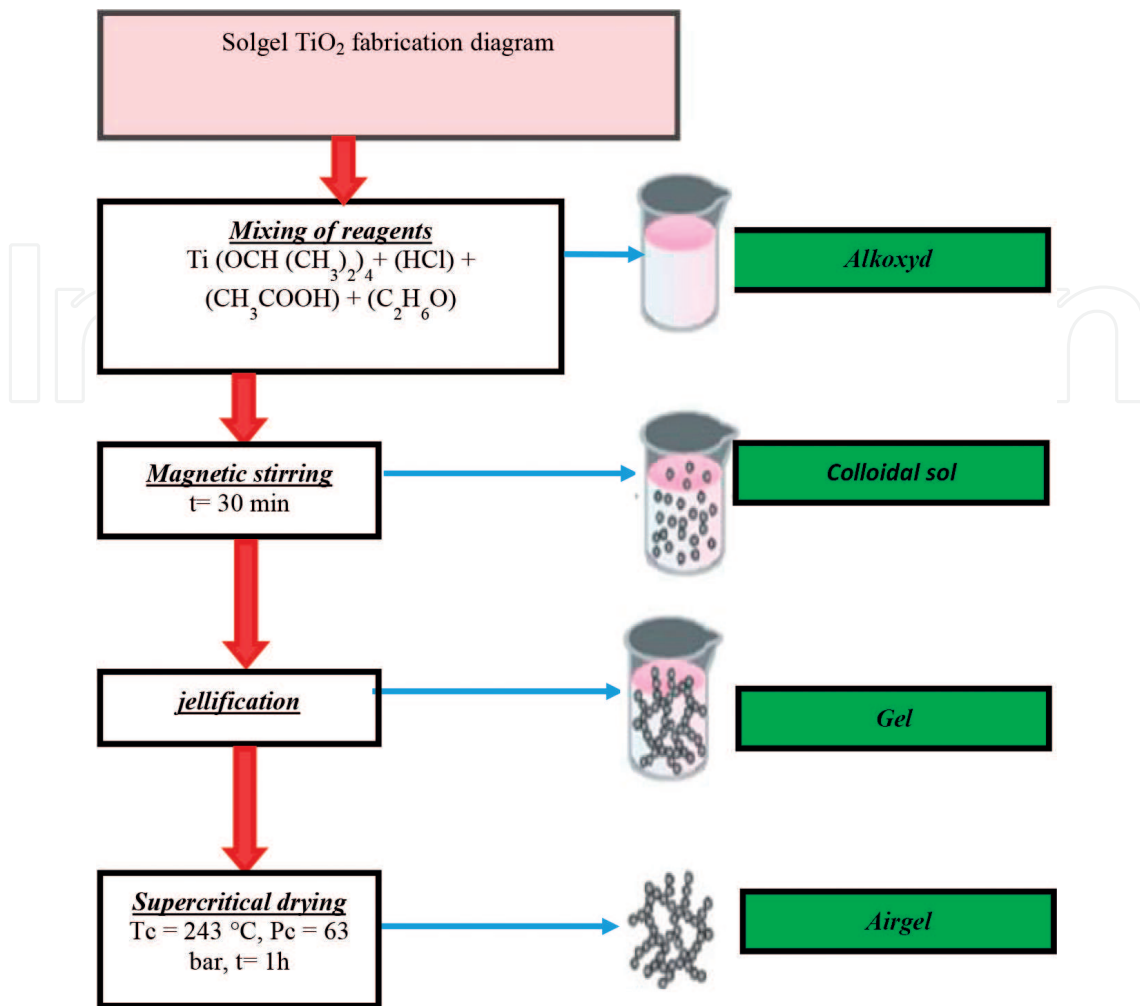
Figure 8. The sol-gel TiO$_2$ fabrication diagram.

2θ (degree) of 25.23, 37.81, and 48.14 degree were indexed as (101), (004), and (200) planes of anatase phase TiO$_2$ which matches well the reported data for TiO$_2$ ((PDF) # 00-021-1272).

The grain size of TiO$_2$ has been calculated using Scherer's equation [9].

With D as the crystallite size of TiO$_2$ thin films, k as a constant (=0.89), λ as the wavelength of X-ray (CuKα = 1.5406 Å), β as the true half-peak width, and θ as the half diffraction angle of the centroid of the peak in degree. Any contributions to broadening due to non-uniform stress were neglected and the instrumental line width in the XRD apparatus was subtracted. The calculated crystallite size of the anatase phase was about 20 nm.

2.3.3. Characterization of synthesized TiO$_2$ nanopowder by SEM and TEM

Figure 11 (a–b) shows the SEM micrographs that describe the morphology of the as-synthe-sized TiO$_2$ nanopowder. As it can be observed from the **Figure 11a**, the powder consists of spherical clusters. In addition, the expertise of **Figure 11b** suggested that the spherical-shaped
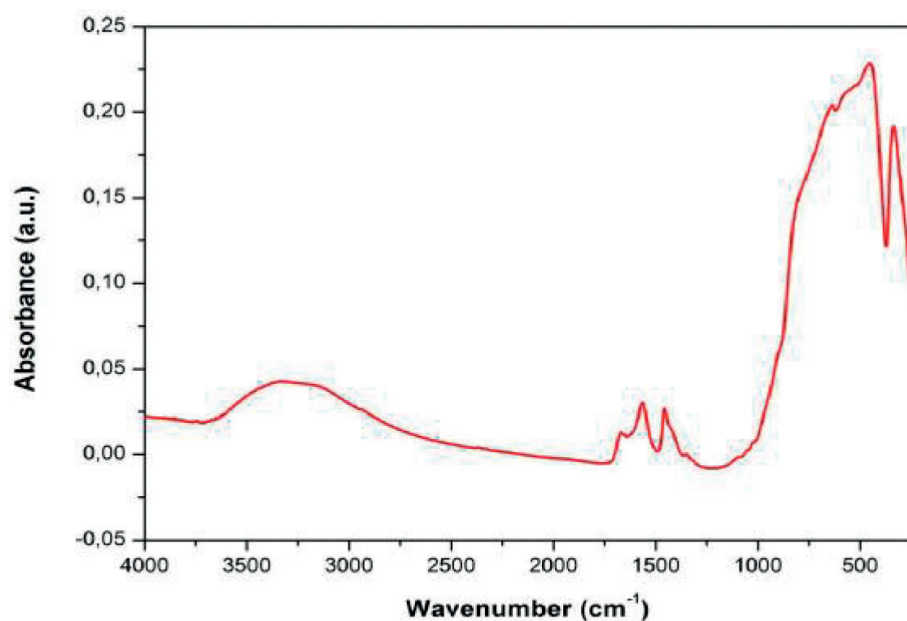
Figure 9. FTIR spectra of as-prepared TiO$_2$ nanopowder.

TiO$_2$ particles are hollow and composed of nanosized TiO$_2$ anatase. The TiO$_2$ nanoparticles show an even distribution with a mean size of about 20 nm.

Furthermore, the crystalline structure of TiO$_2$ nanopowder was investigated by transmission electronic microscopy (TEM) (**Figure 12**) observation in order to estimate the primary TiO$_2$ crystallite. The TEM images of TiO$_2$ nanopowder are shown in **Figure 12 (a–b)**. As shown
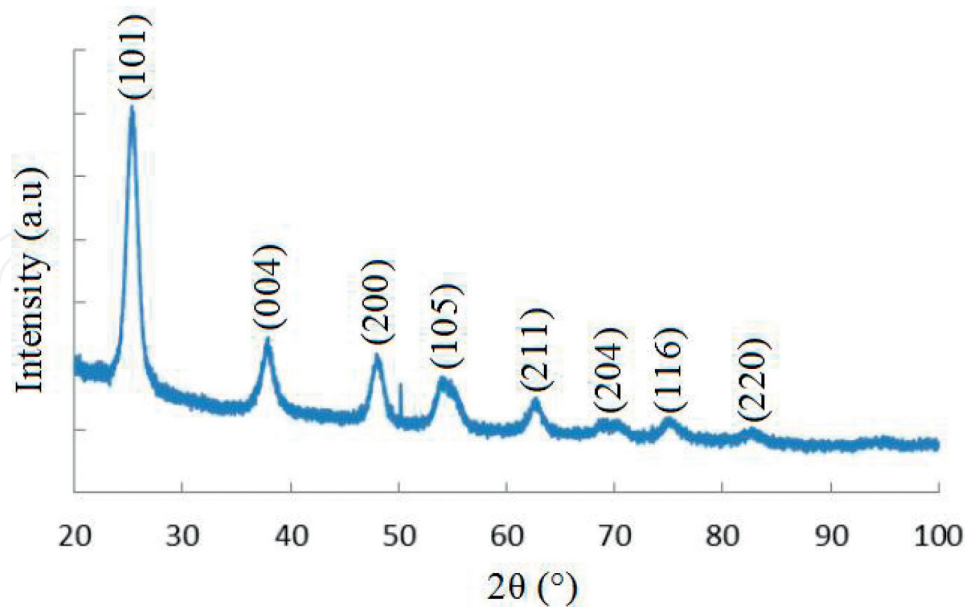
Figure 10. X-ray diffraction pattern of TiO$_2$ nanopowder synthesized by sol-gel process.
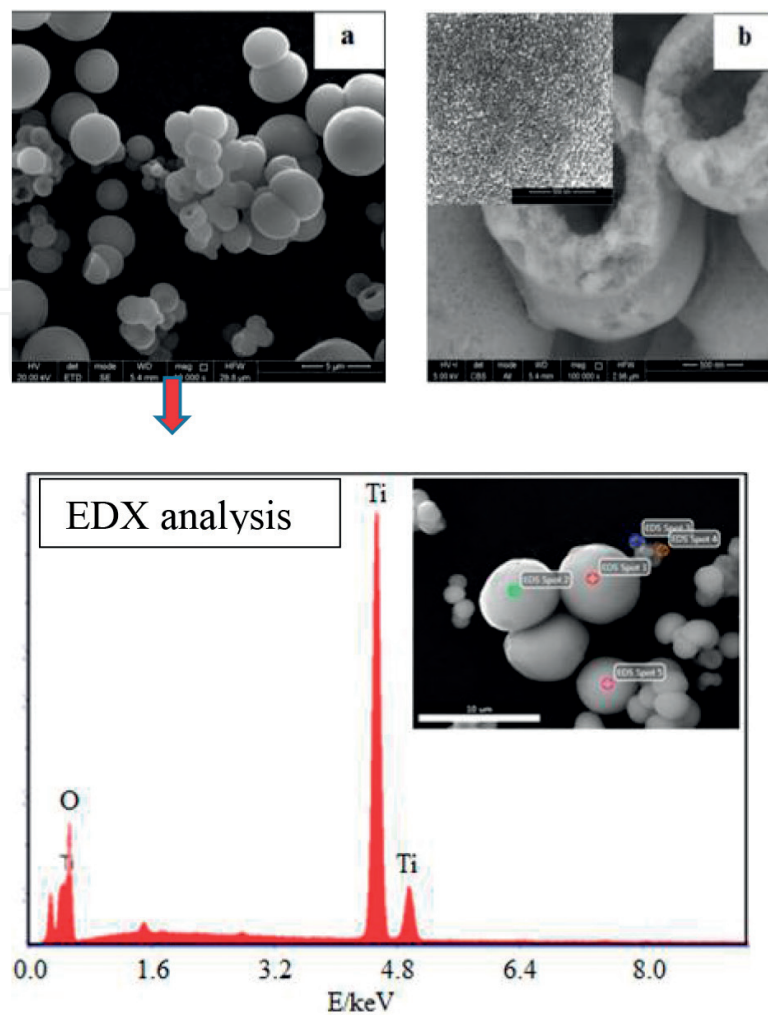
Figure 11. SEM images of synthesized TiO_2 nanopowder (a) Spherical clusters and (b) nanosized TiO_2 anatase.

in **Figure 12a**, the primary TiO_2 crystallite had a diameter of about 10–20 nm which was in a satisfactory agreement with the SEM results.

The local crystal structure of anatase was confirmed by selected area electron diffraction (SAED) technique. One SAED ring diffraction pattern with marked Miller indices of anatase TiO_2 nanopowder (JCPDS card no. 21-1272) is given in **Figure 12b**. The ring pattern confirmed that synthesized nanopowder is polycrystalline with constituent crystallites of about 10 nm or more. Thus from the morphological studies, we can say that the synthesized TiO_2 nanoparticles seemed adequate to be used for the pores filling using an adopted electrophoretic deposition process (EPD).

Energy dispersive X-ray (EDX) spectrometry analysis of the synthetized TiO_2 nanoparticles shows peaks for titanium (Ti) and oxygen (O) elements. There is no trace of any other impurities could be seen within the detection limit of the EDX as presented in **Figure 11**. This indicates that the synthesized TiO_2 nanopowder was qualified with a high purity.

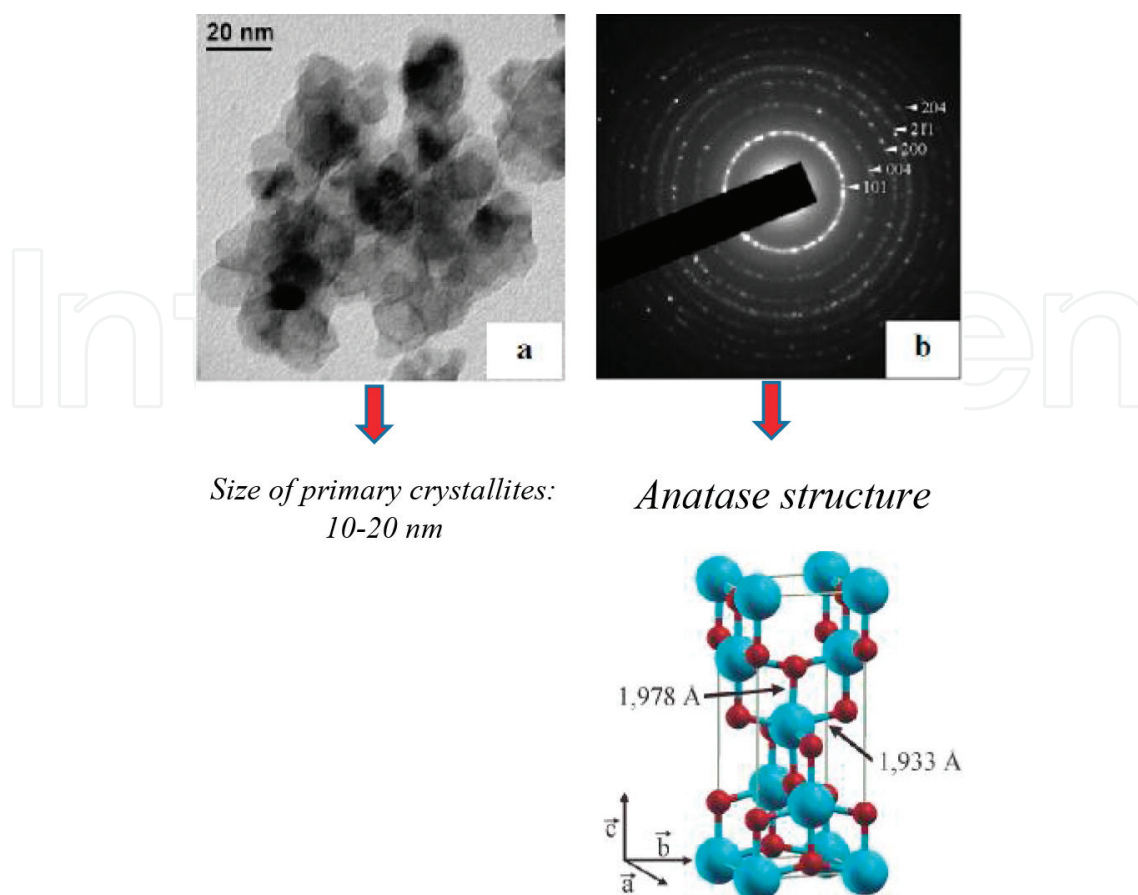*Size of primary crystallites:*
10-20 nm

Anatase structure

Figure 12. Characterization of synthesized nanopowder by SEM (a) Size of primary crystallites and (b) SAED ring diffraction pattern with marked Miller indices of anatase TiO$_2$ nanopowder.

2.3.4. Electrophoretic impregnation of anodizing layer by a synthesized TiO$_2$ nanoparticle

2.3.4.1. Preparation of the TiO$_2$ nanoparticles suspension

2.3.4.1.1. Effect of ultrasound on the dispersion of nanoparticles

According to preliminary studies, 0.05 g/100 ml of TiO$_2$ nanoparticles was chosen as the optimal concentration to achieve the EPD process. To do so, a stock solution (mother solution) that comprises mixing 0.05 g of TiO$_2$ with 100 ml of distilled water was prepared. The mixture was then magnetically stirred for 15 min. To investigate the effect of ultrasound on the dispersion of nanoparticles, the mother solution was subjected to ultrasonic various times (0, 5, 10, 20, 30, 60, and 90 min) (see **Figure 13**). According to the optical properties of the suspension, the absorbance increases with the increase of ultrasonic time. This indicates good dispersion of nanoparticles of TiO$_2$ in the aqueous suspension. Based on the findings shown in **Figure 14**, the use of ultrasound leads to the break of the clusters of TiO$_2$ into smaller agglomerates and aggregates. Agglomerated particles were thus eroded and divided by the collisions between particles [10–12]. A slight difference was observed between 60 and 90 min. So, 1 hour of ultrasonication seemed to be considered as an optimal setting for the preparation of a well-dispersed TiO$_2$ suspension.
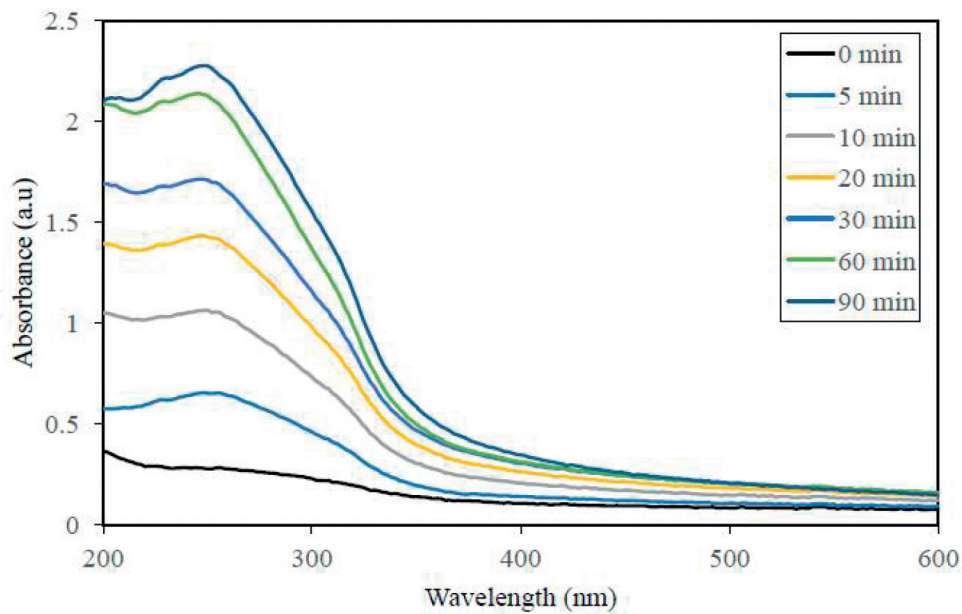
Figure 13. Absorbance spectra of the TiO$_2$ nanoparticles dispersed in water with and without ultrasound as a function of wavelength.
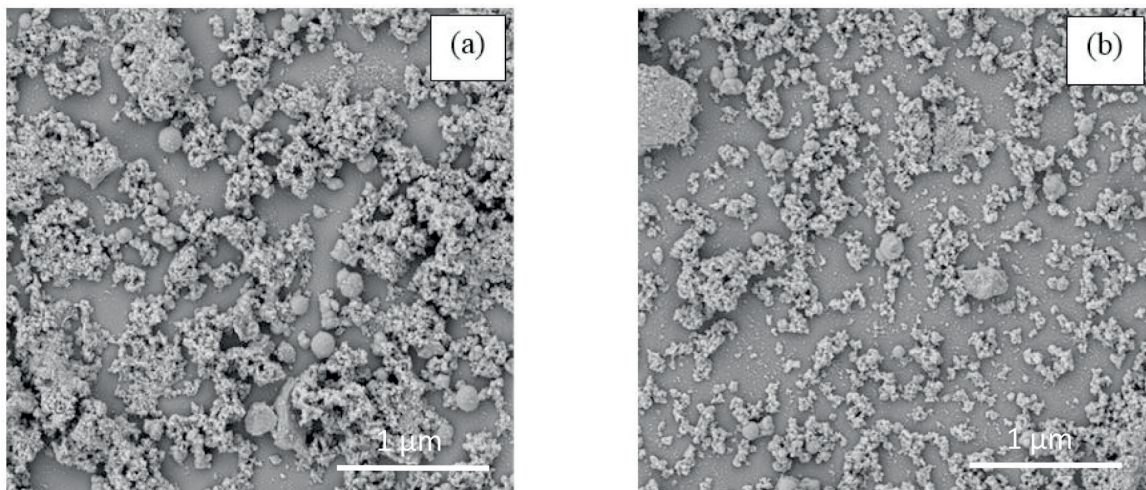

Figure 14. FEG-SEM images of TiO$_2$ nanoparticles: (a) without ultrasound and (b) after 90 min of ultrasound.

2.3.4.1.2. Effect of PAA amount on the zeta potential

Stability of TiO$_2$/poly(acrylic acid) (PAA) suspensions at different polymer content was measured on the basis of zeta potential measurements by means of the electrophoretic mobility. A zeta potential (ζ) of at least 30 mv (positive or negative) was normally required to achieve reasonably stable dispersion [13].

Figure 15 presents the effect of the polymer content on the stability of the suspensions at initial pH (6). According to **Figure 10,** the addition of PAA resulted in a good dispersion of the
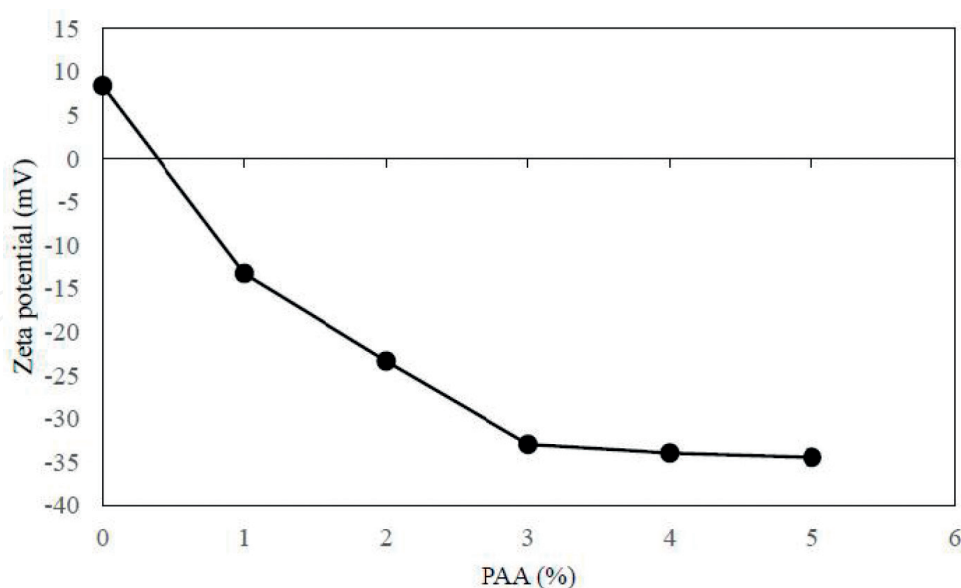
Figure 15. Effect of the amount of PAA on the stability of TiO$_2$ suspension.

suspensions with negative charge. The increase of negatively charged ■COO■ groups was assignable to the modification of the TiO$_2$ nanoparticles surface charge. The addition of 3% PAA was considered as the ideal condition to study and discuss the stability under various pH regions.

2.3.4.1.3. Effect of pH on the zeta potential of the TiO$_2$ suspension

Figure 16 shows the effect of pH on the zeta potential of the TiO$_2$/3% PAA suspension. As the pH increased, the number of negatively charged sites is continually increased until the zeta potential reaches a value over −35 mV at pH ranging between 6 and 8.
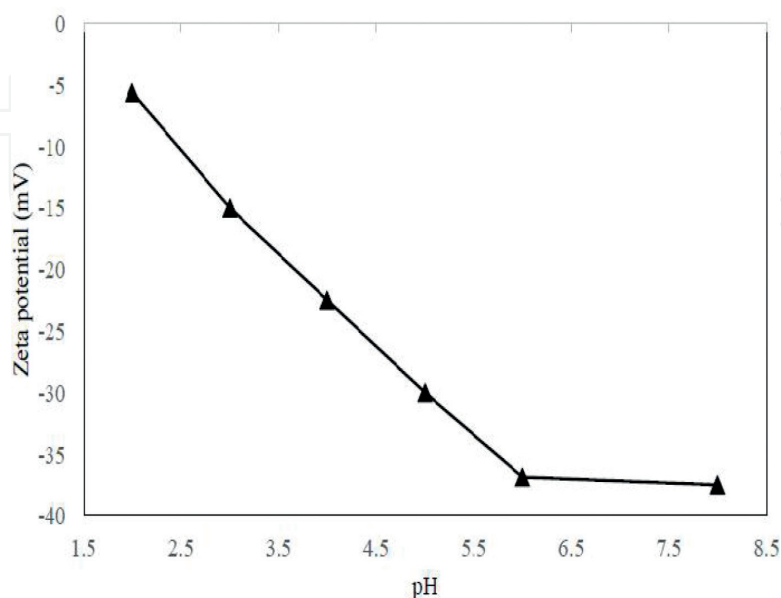

Figure 16. Variation of zeta potential as a function of pH of the TiO$_2$ suspension with 3% PAA.

According to the executed studies, the addition of 3% PAA was considered as the ideal condition and the pH is adjusted at 6.The as-prepared suspension has a zeta potential about −37 mV. So, it is considered a well-stable suspension to carry on electrophoretic process [14].

2.3.4.1.4. Stability of the TiO₂ suspension as a function of sedimentation time

Figure 17 shows the absorbance of titanium dioxide suspensions with and without PAA as a function of sedimentation time. In these tests, the PAA concentration was fixed at 3% and the pH is adjusted at 6. It is observed that the absorbance of titanium dioxide suspensions is lowering as the sedimentation proceeds. It is noteworthy that the absorbance of the suspension in the presence of PAA is stable for at least a week. This means that the adsorbed PAA was expected to provide a degree of electrosteric stabilization. Based on these results, the suspension (3% PAA at pH = 6) was suggested as an optimal standpoint stability to perform the incorporation of TiO₂ nanoparticles into the pores of the anodic oxide using EPD process.

2.3.4.1.5. Electrophoretic impregnation of anodic coating

Electrophoretic impregnation of porous anodizing layer elaborated in phosphoric acid was executed in aqueous TiO₂ nanoparticles suspension. It should be noted that impregnation process is conditioned by the applied electric field. Applying high electric field (200 V/cm) induce the jellification of TiO₂ sol because of the anodic electrolysis of water which decreases the pH near the electrode surface and then destabilize the suspension against coagulation at low pH. In order to avoid this phenomena and facilitate the insertion of titanium dioxide nanoparticles, the addition of the glycine to buffer the suspension is necessary. At the beginning of EPD, particles go to the bottom of pores which continue to fill progressively. These
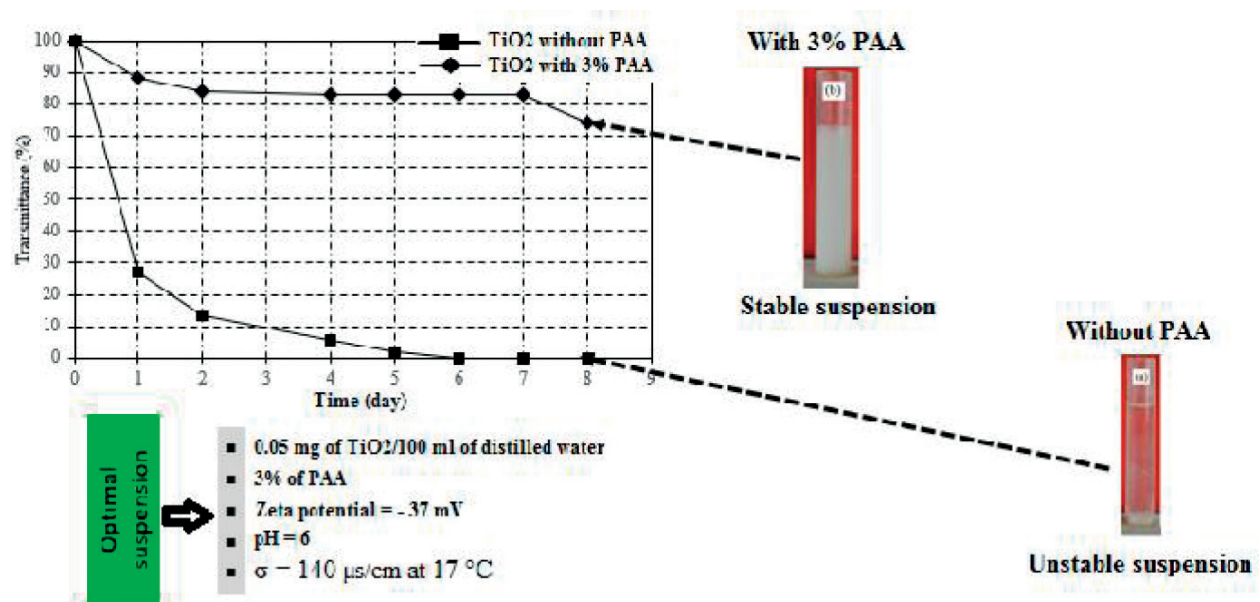

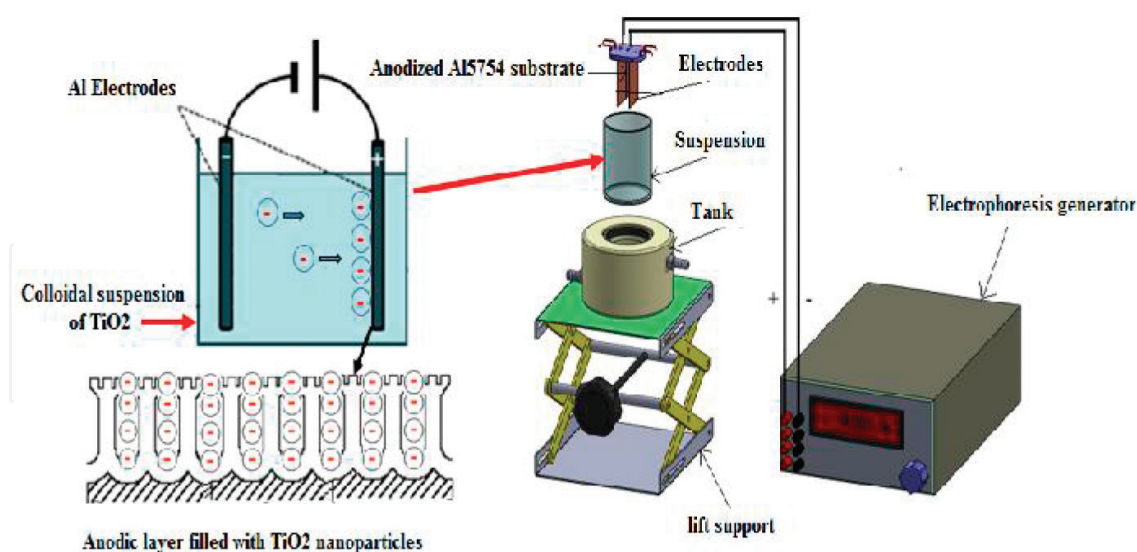**Figure 17.** Variation of transmittance of the TiO₂ suspensions as a function of time.

Figure 18. Experimental setup of electrophoretic impregnation of anodizing layer by a synthesized TiO$_2$ nanoparticle.

results attest that EPD can be used to fill successfully porous-anodizing layer despite the presence of the resistive barrier layer at the metal-oxide interface. **Figure 18** reveals experimental setup of electrophoretic impregnation of anodizing layer by a synthesized TiO$_2$ nanoparticle and the filled anodic layer is shown in **Figure 19**.

As shown in **Figure 19**, an increase of the electric field improves the impregnation depth of nanoparticles. Hence high electric field is necessary here to compensate the resistive
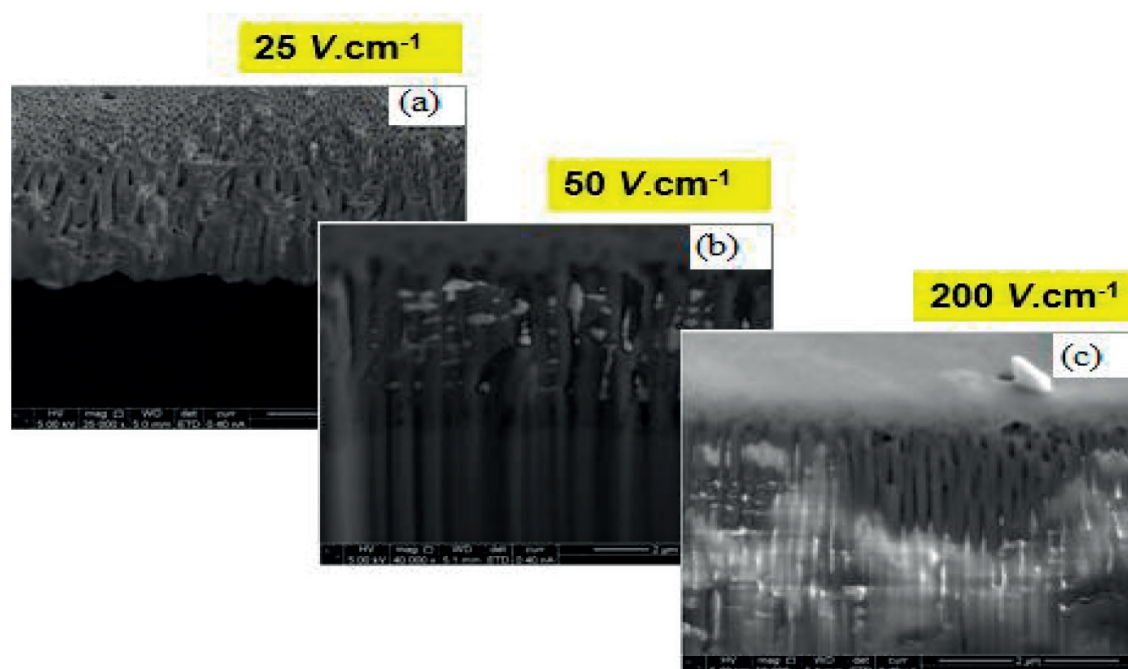

Figure 19. FEG-SEM cross sectional views of the porous anodic oxide: (a) after electrophoresis process using 25 V/cm, (b) after electrophoresis process using 50 V/cm, and (c) after electrophoresis process using 200 V/cm.

barrier layer at the metal-porous anodic film interface [15]. This finding is in satisfactory agreement with that of Fori et al. [15]. The following equation describes the migration speed of the nanoparticles:

$$\nu = \mu E \qquad (1)$$

where ν as the speed of nanoparticles (m/s), μ as the electrophoretic mobility of nanoparticles (m^2/s.V), and E as the electric field (V/m). According to the this equation, an increase of the electric field promotes the driving forces of particles and then facilitates their incorporation inside pores of the anodizing layer.

3. Tribological behavior of Al$_2$O$_3$/TiO$_2$ composite coating

Tribological tests were carried out on a non-anodized aluminum substrate, an anodized coating alone, a composite coating of Al$_2$O$_3$/TiO$_2$ and a TiO$_2$ massive produced by compression of a mass of a TiO$_2$ nanopowder already synthesized by a sol-gel process, in order to study the effect of the incorporation of TiO$_2$ nanoparticles. The results thus obtained bearing essentially on the quantification of friction coefficient and the wear volume are shown in **Figures 20** and **21**, respectively.

Examination of **Figure 20** reveals that the friction coefficient of the anodic coating alone has two periods: (1) a period of 250 seconds (approximately 414 cycles) during which the average friction coefficient fluctuates at about 0.8 and (2) a second period marked by a sharp drop in the friction coefficient until reaching a stable value almost equal to that of the non-anodized
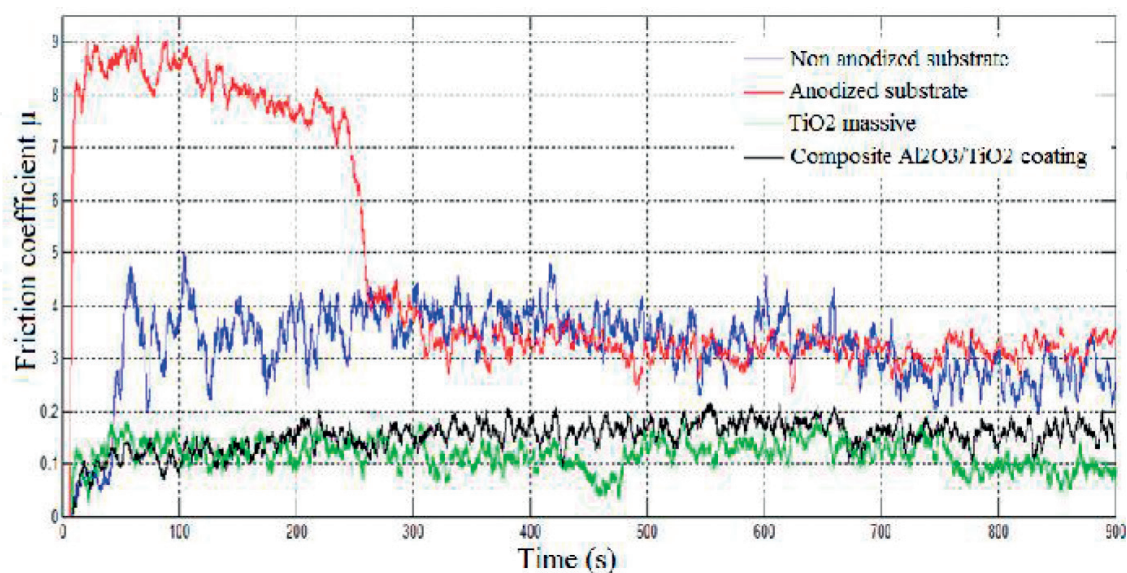

Figure 20. Variation of friction coefficient as a function of time (normal load Fn = 1 N, movement speed v = 0.052 m.s^{-1}, and time of friction t = 15 min).
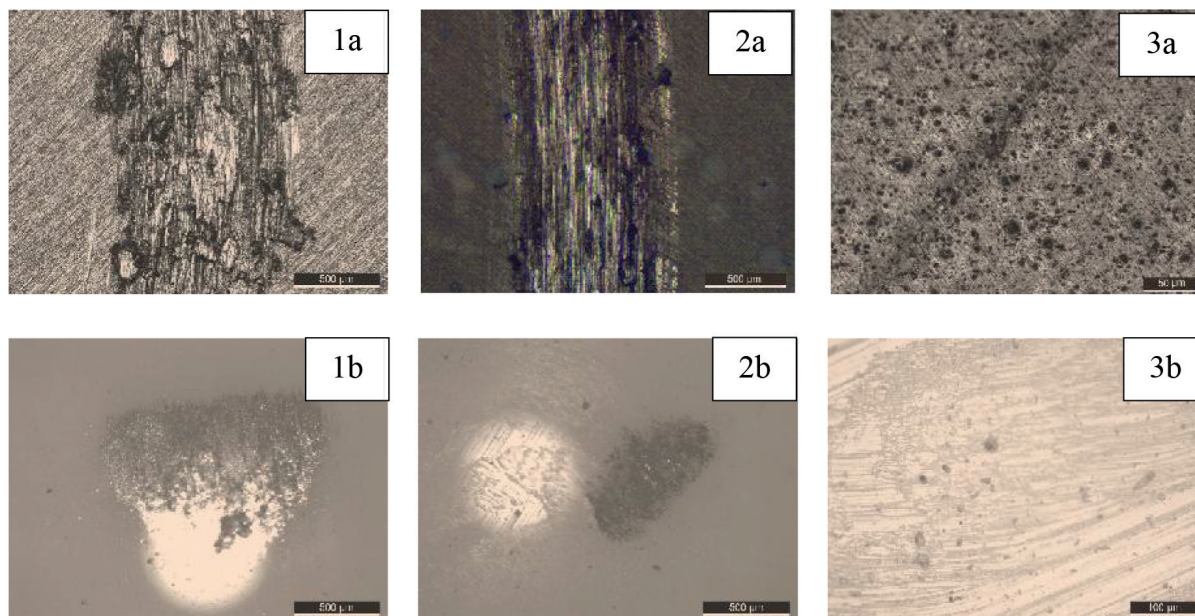
Figure 21. Optical micrographs of (a) the trace and (b) the alumina ball after friction test on (1) non-anodized aluminum, (2) anodic coating alone, and (3) composite coating Al_2O_3/TiO_2 (Fn = 1 N, v = 0,052 ms^{-1} and t = 15 min).

substrate (μ = 0.3). This particular drop of the coefficient of friction indicates the total damage of the anodic coating alone and the alumina ball, constitutes our counterface, then becomes in direct contact with the exposed aluminum. This is confirmed by the optical micrographs of the traces of wear of the ball and the anodic coating alone (**Figure 21**). The anodic coating is totally worn out after 250 seconds (414 cycles) and its trace revealing the substrate and metal debris on the ball.

The TiO_2 massif has a friction coefficient (μ = 0.1) that is practically low throughout the tribological test compared to that of the substrate (μ = 0.30). Optical micrographs of the alumina ball show that TiO_2 arbed on their surfaces (**Figure 21 (2b)** and **Figure 16 (b)**).

At this level, we can partially conclude that after measuring the friction coefficient of the aluminum alloy (μ = 0.3), the anodic coating alone and the TiO_2 massif (μ = 0.1), it was therefore possible to evaluate the coefficient of friction and the lifetime of the anodic coating alone (μ = 0.8 and a lifetime = 414 cycles).

The curve reflecting the variation of the coefficient of friction of the composite anodic coating Al_2O_3/TiO_2 as a function of time evolves in two periods: (1) a first period (at approximately 100 seconds) during which the coefficient of friction is almost equal to that of the solid mass TiO_2 (μ = 0.1) and (2) a second period (the rest of the friction test) during which the coefficient of friction increases slightly until reaching an almost stable value (μ = 0.15). These two periods respectively correspond to the ball contacts of alumina/TiO_2 deposited on the surface of the anodic coating and ball of alumina/composite coating.

It should be noted that the composite anodic coating will end up with a mean friction coefficient μ = 0.15, intermediate between that of the TiO_2 massive (μ = 0.1) and that of the non-anodized
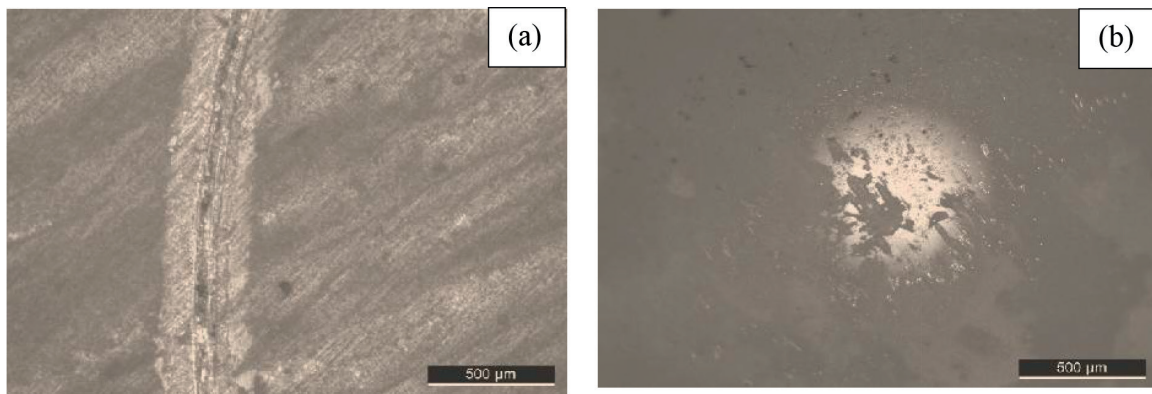
Figure 22. Optical micrographs (a) trace of wear of a TiO$_2$ solid and (b) trace of wear of the counterface (alumina ball) after friction test (Fn = 1 N, v = 0.052 m.s^{-1} and t = 15 min).

substrate (μ = 0.30) without causing a sudden variation. This reflects that this coating still persists in wear and has a lifetime greater than 900 seconds (1490 cycles). The optical image shown in **Figure 22 (3a)** shows that the composite coating has low wear free of microcracks. While, the counterface (**Figure 21 (3b)**) does not show either TiO$_2$ or oxide.

The characteristics of the wear traces of the various samples thus examined are measured and the volume of wear is calculated (**Figure 23**). The expertise of the latter figure shows that the TiO$_2$ massive has a low wear volume (29.6106 μm^3) intermediate between that of the substrate (461.4106 μm^3) and that of the anodic coating alone (373,106 μm^3). Such a coefficient of friction (μ = 0.1) and a low wear volume justify a credible choice of TiO$_2$ nanoparticles to be used

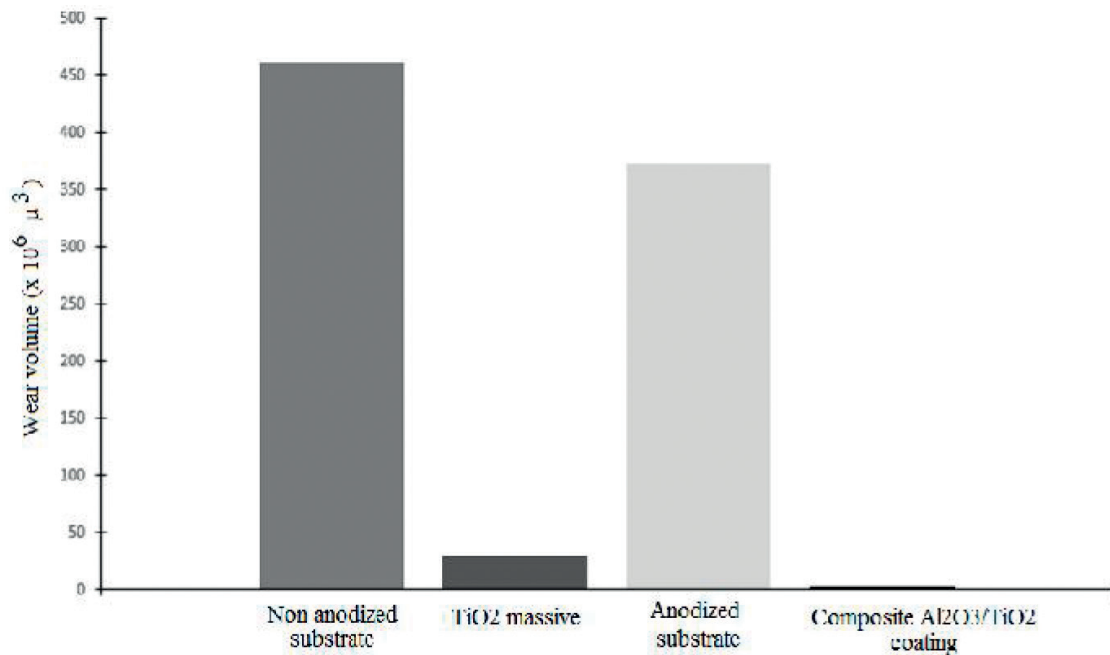**Figure 23.** Variation of the wear volume of the worn samples after friction tests (Fn = 1 N, v = 0.052 m.s^{-1} and t = 15 min).

for the electrophoretic impregnation of the anodic coating developed in a phosphoric bath in order to reinforce its tribological behavior.

The composite anodic coating, as shown in **Figure 23**, has a wear volume (3.4106 μm^3) which has 0.73% of that of the substrate and about 0.91% of that of the anodic coating alone.

Finally, this panoply of the results confirms that the functionalization of the anodic coating by TiO_2 nanoparticles contributes to a significant improvement in its resistance to frictional wear.

These results are in satisfactory agreement with those found by Yugeswaram et al. [16] in the case of an Al_2O_3/13% TiO_2 composite coating developed by the Air Plasma Spray (APS) process.

4. Conclusion

Electrophoretic impregnation of porous anodizing layer elaborated in phosphoric acid was executed in aqueous TiO_2 nanoparticles suspension. It should be noted that impregnation process is conditioned by the applied electric field. Applying high electric field (200 V/cm) induces the jellification of TiO_2 sol because of the anodic electrolysis of water which decreases the pH near the electrode surface and then destabilizes the suspension against coagulation at low pH. In order to avoid this phenomenon and facilitate the insertion of titanium dioxide nanoparticles, the addition of the glycine to buffer the suspension is necessary. At the beginning of EPD, particles go to the bottom of pores which continue to fill progressively.

These results attest that EPD can be used to fill successfully porous anodizing layer despite the presence of the resistive barrier layer at the metal-oxide interface.

Author details

Koubaa Anouar* and Bargui Mansour

*Address all correspondence to: anouar.koubaa@gmail.com

High Institute of Technological Studies of Sfax, Tunisia

References

[1]   Bal S, Samal SS, Mohanty UK. Mechanical and microstructural analysis of carbon nanotube composites pretreated at different temperatures. American Journal of Materials Science. 2011;**1**(1):5-11. DOI: 10. 5923/j.materials.20110101.02

[2]   Sulka GD, Stroobants S, Moshchalkov V, Borghs G, Celis J-P. Synthesis of well-ordered nanopores by anodizing aluminium foils in sulfuric acid. Journal of the Elechtrochemical Society. 2002;**149**(7):D97-D103

[3] Seventy Years of Sulfuric Acid Anodizing-Brace-Trans MFI; 1997

[4] O'Sullivan JP, Wood GC. The morphology and mechanism of formation of porous anodic films on aluminium. The Royal Society's Physical Sciences Research Journal. 1970;**317** (1531). DOI: 10.1098/rspa.1970.0129

[5] Bargui M, Messaoud M, Elleuch K. Electrophoretic impregnation of porous anodizing layer by synthesized TiO_2 nanoparticles. Surface Engineering and Applied Electrochemistry. 2017;**53**(5):467-474. DOI: 10.3103/S1068375517050040

[6] Han LS, Rujkorakarn R, Sites JR, Ske CY. Thermally induced crystallization of amorphous-titania films. Journal of Applied Physics. 1986;**59**:3475. doi.org/10.1063/1.336817

[7] Fitzgibbons ET, Sladek KJ, Hartwig WH. TiO_2 film properties as a function of processing temperature. Journal of the Electrochemical Society. 1972;**119**:753. DOI: 10.1149/1.2404316735-739

[8] Cozzoli PD, Kornowski A, Weller H. Low-temperature synthesis of soluble and processable organic-capped anatase TiO_2 nanorods. The American Journal of Chemical Society. 2003;**125**:14539-14548. DOI: 10.1021/ja036505h

[9] Cullity BD. Elements of X-ray diffraction. Reading, Mass. Addison-Wesley; 1956. 514 p. (OCoLC)904102259

[10] Sato K, Li JG, Kamiya H, Ishigaki T. Ultrasonic Dispersion of TiO_2 Nanoparticles in Aqueous Suspension. American Journal of Ceramic Society. 2008;**91**(8):2481-2487. doi.org/10.1111/j.1551-2916.2008.02493.x

[11] Sato K et al. Ultrasonic dispersion of TiO_2 nanoparticles in aqueous suspension. Journal of the American Ceramic Society. 2008;**91**(8):2481-2487

[12] Escabor J, Arurault L, Turq V. Improvement of the tribological behavior of PTFE-anodic film composites prepared on 1050 aluminium substrate. Applied Surface Science. 2012;**258**:8199-8208. DOI: 10.1016/j.apsusc.2012.05.022

[13] Malvern Instrument – Zeta potential: An introduction in 30 minutes – Technicalnote MRK654-01

[14] Zeta Potential: An Introduction in 30 Minutes, Technical Note MRK654-01. Malvern Instrum: Malvern; 2017

[15] Fori B, Taberna PL, Arurault L, Bonino JP, Gazeau C, Bares P. Electrophoretic impregnation of porous anodic aluminum oxide film by silica nanoparticles. Colloids and Surfaces, A: Physicochemical and Engineering Aspects. 2012;**415**:187-194. DOI: 10.1016/j.colsurfa.2012.09.011

[16] Yugeswarana S, Selvarajana V, Vijaya M, Ananthapadmanabhanb PV, Sreekumarb KP. Influence of critical plasma spraying parameter (CPSP) on plasma sprayed alumina–titania composite coatings. Ceramics International. 2010;**36**:141-149. DOI: 10.1016/j.ceramint.2009.07.012